Reaction Kinetics, Mechanisms and Catalysis (2021) 134:727–742
https://doi.org/10.1007/s11144-021-02090-w

Kinetic modeling of CuO/CeO_2 and CuO/Nb_2O_5 as oxygen carriers in the production of syngas

Hassan A. Saddiq[1,2] · Ibrahim A. Muhammed-Dabo[1] · Abba Hamza[1] · Saidu M. Waziri[1]

Received: 14 June 2021 / Accepted: 12 October 2021 / Published online: 27 October 2021

Abstract

Oxygen carriers such as CuO/CeO_2 and CuO/Nb_2O_5 were found to have very good selectivity to syngas products when used in chemical looping reforming. The oxygen carriers with 10% CuO has been applied in partially oxidizing liquefied petroleum gas in a chemical looping reforming process at 800 °C and the kinetic model of the processes were developed and then validated with the experimental data. The results show that first order kinetic, 3D contraction and third order kinetic models gave best fits for CuO/CeO_2 powder, CuO/CeO_2 pellets and CuO/Nb_2O_5. These resulted in rate constants of 0.0836 s^{-1}, 0.0202 s^{-1}, 0.1075 s^{-1} and 0.0682 s^{-1} for CuO/CeO_2 powder, CuO/CeO_2 pellets, CuO/Nb_2O_5 powder and CuO/Nb_2O_5 pellets. Using the rate constants, the model results were found to give good correlations when compared to experimental data.

Keywords Syngas · Chemical looping · Kinetic model · CuO · CeO_2 · Nb_2O_5

Introduction

Syngas is a gaseous fuel consisting of H_2 and CO [1–4] which can be produced using different conventional processes such as partial oxidation, steam reforming and chemical looping reforming [5, 6] in which hydrocarbon molecule in a fuel are broken down by introduction of oxygen [7]. Syngas is an important component in the production of many fuel and chemicals such as hydrogen, methanol and Fischer Tropsch products [4, 8, 9] which are very essential in chemical industries.

Chemical looping is a novel technology that uses metal oxides called oxygen carrier for the transfer of both material and energy between two or more reactors for the

✉ Hassan A. Saddiq
kabsaddiq@mautech.edu.ng

[1] Department of Chemical Engineering, Ahmadu Bello University, Zaria, , Kaduna State, Nigeria

[2] Department of Chemical Engineering, Modibbo Adama University, Yola, Adamawa State, Nigeria

oxidation of fuel with the aim of optimizing material and energy distribution [10]. There are oxidation–reduction processes between the oxygen carrier and the fuel [11] which takes place in an air and a fuel reactors [10, 12, 13]. The reaction in the air reactor is highly exothermic while that in the fuel reactor can either be endothermic or exothermic depending on the metal oxide used [10, 14–17]. Chemical looping can be applied in different forms depending on the intended products required from the process, i.e. either to obtain energy with basic products being CO_2 and H_2O (chemical looping combustion) [18–20] or to partially oxidize the fuel thereby producing syngas (chemical looping reforming) [1, 4, 21, 22] as indicated in reactions R1–R3 [16, 23, 24].

$$Me_xO_{y-1} + \frac{1}{2}O_2 \rightarrow Me_xO_y \tag{R1}$$

$$(2n+m)Me_xO_y + C_nH_{2m} \rightarrow (2n+m)Me_xO_{y-1} + mH_2O + nCO_2 \tag{R2}$$

$$Me_xO_y + C_nH_{2m} \rightarrow Me_xO_{y-n} + mH_2 + nCO \tag{R3}$$

Here Me_xO_y is the oxidized form of the oxygen carrier while Me_xO_{y-1} is the reduced form of the oxygen carrier, C_nH_{2m} is the fuel used.

The task of obtaining the desired product can be achieved by selecting a suitable oxygen carrier that can oxidize the fuel either fully or partially [14, 15]. The redox behavior of an oxygen transfer material which can have significant effect on the system performance is highly dependent on the thermochemical properties of the metal oxide [25]. Thermodynamics consideration shows that metal oxides are grouped into three zones which can be used for complete combustion, partial oxidation or as an inert material (support) in chemical looping as demonstrated in Ellingham diagram [26].

Some of the materials in the zone for complete combustion such as CuO, Mn_2O_3 and Co_2O_3 are reported to be very reactive due to their oxygen uncoupling characteristics at a temperature of 850 °C [8, 26, 27] and CuO was reported to be the most reactive [28–30] but degrades quickly when used alone [31]. Meanwhile CeO_2 and Nb_2O_5 are reported to be good metal oxides for use in partial oxidation of fuel in chemical looping as can be seen on Ellingham diagram [26]. Even though they have high selectivity to syngas generation in chemical looping and can therefore be used as chemical looping reforming oxygen carrier, they are found to have low reactivity when used alone at moderate temperature of between 800 °C and 900 °C [3, 17, 32, 33]. It was observed that partial oxidation of methane to syngas can be achieved by addition of only 1% Pt at a temperature of 600–800 °C but with low reactivity [34] and it was also reported that with use of support, there is high selectivity to syngas at a temperature of 870 °C and the support that gives the highest selectivity was found to be Al_2O_3 [35] but it was found that there is reduction in reactivity with increase in CeO_2 composition in the oxygen carrier [36].

Due to high selectivity of CeO_2 and Nb_2O_5 oxygen carriers to syngas, attempts has been made by numerous researchers to combine the metal oxide with some other metal oxides that are highly reactive for the purpose of having products

with high selectivity to syngas. He et al. (2009) [3] reported methane conversion of around 70% with CO and H_2 Selectivity of around 90% using CeO_2/Fe_2O_3 at a temperature of 850 °C meanwhile Yan et al. (2018) [17] reported maximum conversion of around 85% and maximum selectivity of around 50% for CO and 70% for H_2 using the same oxygen carrier and at the same condition. On the other hand Li *et* al. (2010) [37] and Li *et* al. (2011) [38] reported methane conversion of around 90% and selectivity of around 95% for CO and H_2 when using CeO_2/Fe_2O_3 oxygen carrier with 70% and 80% CeO_2 at a temperature of 900 °C meanwhile Gu et al. (2013) [6] reported methane conversion of about 25.5% with CO and H_2 selectivity of about 90% when CeO_2/Fe_2O_3 oxygen carrier with 80% CeO_2 was used at the same condition. There was also a report by dos Santos et al. (2019) [39] that using 5% Nb_2O_5 in Nb_2O_5/Al_2O_3 at a temperature of 900 °C, conversion of around 90% was obtained but selectivity of CLR products was only 20% at the end of 6 min of operation. It was also reported that when CeO_2 and Nb_2O_5 were combined, there was syngas production from methane at a temperature of between 900 K and 1000 K but it was observed that there was re-oxidation of the hydrogen to form water and consequently, the products of the reaction are mainly CO and H_2O [40]. Wei et al. (2010) [41] reported methane conversion of 48.80% and selectivity of 86.67% and 88.90% for H_2 and CO, respectively, at 800 °C when CeO_2/NiO oxygen carrier with 90% CeO_2 composition was used. There was also a report that methane conversion using 50% CuO/CeO_2 oxygen carrier at a temperature of 850 °C gave about 95% selectivity of CO but there was observed methane decomposition at that temperature [3].

For a kinetics model, mathematical expressions can be employed to express relationship between the conversion of a given component and time of reaction which is the rate of change of conversion [42]. Since chemical looping involves a reaction between gas and solid, a gas–solid expression is required to obtain a model that describes the system. For a gas–solid reaction, the rate can be controlled by various mechanisms, so there are various models that can be used to describe the mechanism which include kinetic controlled model, diffusion controlled model, phase boundary controlled model and nucleation and growth controlled model [1, 43]. The rate of solid conversion of such a system can simply be written in term of the reaction model and the kinetic rate constant [42], so rate of conversion of oxygen carrier can be written as follows.

$$\frac{dX}{dt} = k(T)f(X) \tag{1}$$

Here $k(T)$ is the rate constant and follows Arrhenius expression as;

$$k(T) = k_{01} \exp\left(\frac{-E}{R}\left(\frac{1}{T} - \frac{1}{T_0}\right)\right) \tag{2}$$

k_{01} is the pre-exponential factor, E is the Activation energy, T and T_0 are the temperature of operation and the reference temperature while R is the gas constant.

There are various reaction models given for solid state decomposition and for model expression in Eq. 1, f(X) have been given in literature [42–45]. For an

experimental data that is generated isothermally, the model function can be integrated to obtain an expression shown in Eq. 3 [42].

$$g(X) = \int_0^X \frac{dX}{f(X)} = k(T)t \tag{3}$$

It has been widely reported that for an appropriate model describes the experimental data, plotting the above function can yield a straight line with the slope being the rate constant [42–45] but using this method has been found to be inappropriate as it may give parameters that are not application in actual applications [46] giving rise to force fitting [47]. In this case, the expressions will be evaluated with respect to the dependent variable for use in MATLAB for calculating its values, meanwhile for pseudo first order kinetics, an excel file suitable for use can be found at http://lenteg.ttk.pte.hu/KinetFit.html. Statistical methods described by Lente (2015) [47] is found appropriate for calculating standard error given by the expression in Eq. 4.

$$\sigma c_i = \sqrt{\frac{\underline{\underline{M}}^{-1} S\left(C_1, C_2, C_3, \ldots . C_m\right)}{N - m}} \tag{4}$$

Here $\underline{\underline{M}}^{-1}$ is the inverse of matrix of derivatives of the function with respect to the parameters, C_i is a parameter, N is the number of data points, m is the number of parameters, $S(C_1, C_2, \ldots..C_m)$ is the sum of squares error.

The kinetics of many oxygen carriers in chemical looping have been modeled but the kinetics model for CuO/CeO_2 and CuO/Nb_2O_5 oxygen carriers in chemical looping reforming has not been reported in open literature, so there is need to device model expressions that will describe chemical looping reforming using the oxygen carriers.

Experimental procedure

Oxygen carrier preparation

For the preparation of CuO/CeO_2 oxygen carrier using coprecipitation method, the precursors were Copper (II) nitrate trihydrate ($Cu(NO_3)_2.3H_2O$) and cerium (IV) nitrate hexahydrate ($Ce(NO_3)_3.6H_2O$) both obtained from FamousChem, China, while the precipitating agent was ammonium hydroxide (NH_4OH) purchased from a chemical shop in Samaru, Zaria. The two precursors were dissolved in distilled water making up 350 g/l [48] in such a way to obtain CuO/CeO_2 oxygen carrier with 10% CuO. The solution was heated to a temperature of 80 °C while stirring vigorously and adding the NH_4OH in drops to adjust the pH to between 8.0 and 9.5 so as to form precipitate. It was then aged for further 2 h while heating under the same temperature and stirring, after which the precipitate was filtered and washed for about 4 to 5 times using distilled water. The precipitate was then air dried for 24 h before being dried in an oven at a temperature of 110 °C for another 5 h after

which it was crushed using mortar to form powder. Part of the powder was mixed with distilled water and starch [49, 50] to form paste which was then extruded in a syringe, cut into small pieces to form pellets and then dried in an oven at a temperature of 110 °C for 5 h. The material was then calcined at a temperature of 600 °C for 2 h and then at a temperature of 900 °C for further 3 h to obtain powder and pellets oxygen carrier.

To prepare 10% CuO/Nb_2O_5 oxygen carrier, the precursor $Ce(NO_3)_3{\cdot}6H_2O$ was changed with Nb_2O_5 also obtained from FamousChem which was dissolved in 40% hydrofluoric acid by heating it at a temperature of 100 °C for 4 h before being mixed with the other precursor.

Characterization of the oxygen carrier

The oxygen carrier was characterized using x-ray powder diffraction (XRD) pattern using 2θ angle range of 0° to 75°.

Reactivity studies

The reactivity of the oxygen carrier with the fuel was studied using a fixed bed reactor with 12 mm internal diameter and a length of 400 mm as illustrated in Fig. 1.

Three grams of the oxygen carrier was loaded into the fixed bed reactor in each case; which is placed between coarse sand to enhance the distribution of the air/fuel and the bed was heated to a temperature of 800 °C in the flow of nitrogen (N_2)

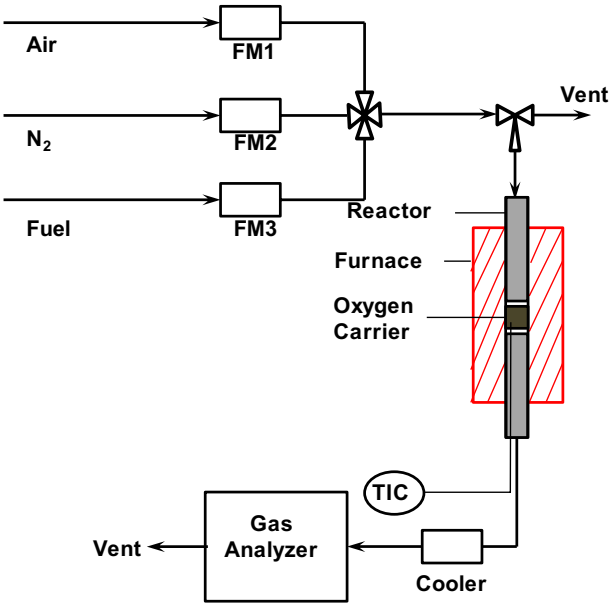

Fig. 1 Illustration of a fixed bed reactor setup for reactivity studies

at 200 ml/min to create a neutral atmosphere in the reactor. Air was then passed through it at a flow rate of 200 ml/min to oxidize the oxygen carrier for a period of 5 min after which Liquefied petroleum gas (95% normal butane and 5% propane LPG) was passed through the bed together with nitrogen at a flow rate of 300 ml/min in a ratio of 1:2 to be oxidized by the oxygen carrier. The product was then analyzed using Hubei RS232 gas analyzer to determine the composition of the products.

Analyses of data and model presentation

Conversion of the fuel can be obtained by using the following reactions [51, 52];

$$C_3H_8 + 3Me_xO_y \rightarrow 3CO + 4H_2 + 3Me_xO_{y-1} \tag{R4}$$

$$C_4H_{10} + 4Me_xO_y \rightarrow 4CO + 5H_2 + 4Me_xO_{y-1} \tag{R5}$$

And the conversion can be calculated using the following expressions;

$$Conversion = \frac{Fuel\ \text{Consumed}}{Fuel\ \text{In}} \times 100\% \tag{5}$$

$$C_3H_{8,Consumed} = nCO + nCO_2 + \tfrac{1}{4}\left(nH_2 - 4nCO\right) \tag{6}$$

$$C_4H_{10,Consumed} = nCO + nCO_2 + \tfrac{1}{5}\left(nH_2 - 5nCO\right) \tag{7}$$

$$Fuel\ \text{Consumed} = 0.05 \times C_3H_{8,Consumed} + 0.95 \times C_4H_{10,Consumed} \tag{8}$$

Oxygen carrier conversion can be calculated using the following expression [48];

$$X_{Oxygen\ carrier} = \frac{R_{CO_2}\sum nCO_2 + R_{CO}\sum nCO}{Total\ mole\ of\ oxygen\ in\ oxygen\ carrier} \tag{9}$$

Here R_i is the stoichiometric ratio of the oxygen carrier to component i while $\sum ni$ is the summation of the moles compositions of component i.

The system is modeled based on the kinetic expression presented in Eq. 6 where model expressions presented in literature [44, 45, 53] are tested to obtain the model with the best fit where it is expected to minimize the standard error from the parameters and the sum of squares errors from the data points and the model results [47]. Since only one parameter is required in this case, the standard error is calculated using the modified form of the expression presented by [47] as follows;

$$\sigma c_i = \sqrt{\frac{\left(\frac{\partial f(t)}{\partial k}\right)^{-1} S(k)}{N-1}} \tag{10}$$

Various models tested are presented in Table 1.

Table 1 Kinetic models selected for use in this work

Kinetics Model	g(X)	Evaluated as
First Order Kinetic Model	$-\ln(1-X)$	$X=1-\exp(-kt)$
1.5 Order Kinetic Model	$2((1-X)^{-1/2}-1)$	$X=1-1/((kt)/2+1)^2$
2nd Order Kinetic Model	$(1-X)^{-1}-1$	$X=1-1/(k(t+1))$
3rd Order Kinetic Model	$2((1-X)^{-2}-1)$	$X=1-[2(1/(kt+2))]^{1/2}$
3D Contraction Model	$[1-(1-X)^{1/3}]$	$X=(kt-1)^3+1$
1.5 Order Nucleation Model	$[-\ln(1-X)]^{2/3}$	$X=1-\exp(-(kt)^{3/2})$
3D Gingstein-Brounstein Model	$(1-2/3X)+(1-X)^{2/3}$	$t=1/k((1-2/3X)+(1-X))^{2/3}$

Results and discussion

Oxygen carrier characterization

The oxygen carrier was characterized using x-ray powder diffraction (XRD) and the images for CuO/CeO_2 and CuO/Nb_2O_5 oxygen carriers are shown in Fig. 2.

From the XRD images, clear peaks of CuO as compared to those of [27, 54], CeO_2 as compared to those of [22, 55] and Nb_2O_5 as compared to those of [56, 57] can be clearly seen which is an indication that the materials are crystal in nature since amorphous materials have XRD images with diffuse intensity. The crystalinity of the materials were obtained due to high calcination temperature used because it has been reported that high temperature of calcination leads to crystalline materials [58]. When the XRD peaks of the oxygen carrier with 10% CuO was compared with those of CuO and CeO_2 in CuO/CeO_2 oxygen carrier, CuO and Nb_2O_5 in CuO/Nb_2O_5 oxygen carrier, it can be seen that the peaks formed are the reflections from those of CuO and CeO_2 and CuO and Nb_2O_5, which is an indication that there were no extra materials formed as a result of interaction between the two materials. Therefore the only materials involved

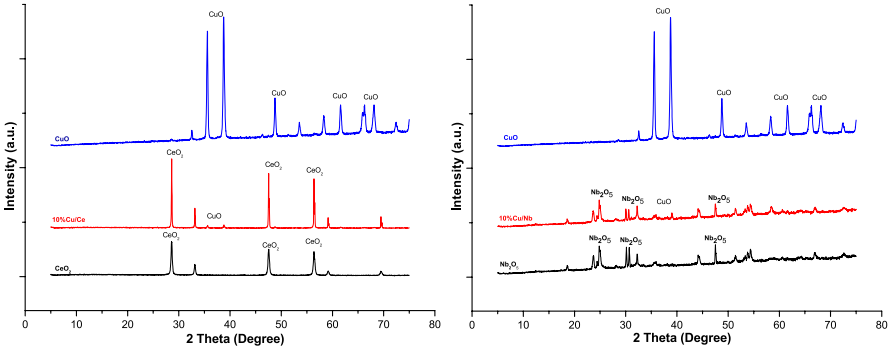

Fig. 2 XRD images for CuO/CeO_2 and CuO/Nb_2O_5 oxygen carriers for CuO, CeO_2 and 10% CuO/CeO_2 on left and CuO, Nb_2O_5 and 10% CuO/Nb_2O_5 on the right

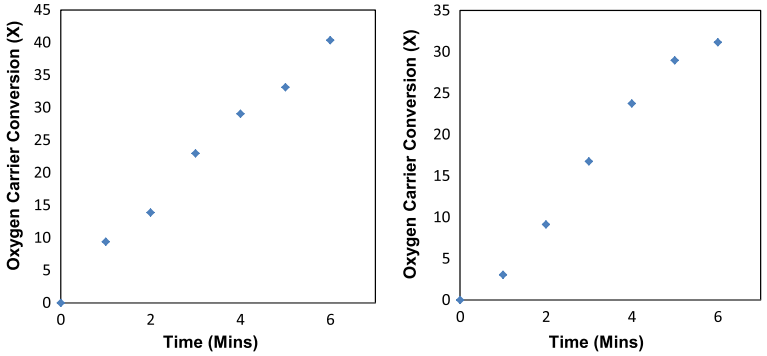

Fig. 3 Experimental result for rate of oxygen carrier conversion for CuO/CeO_2 powder on left and pellets on right performed at 800 °C for a period of 6 min

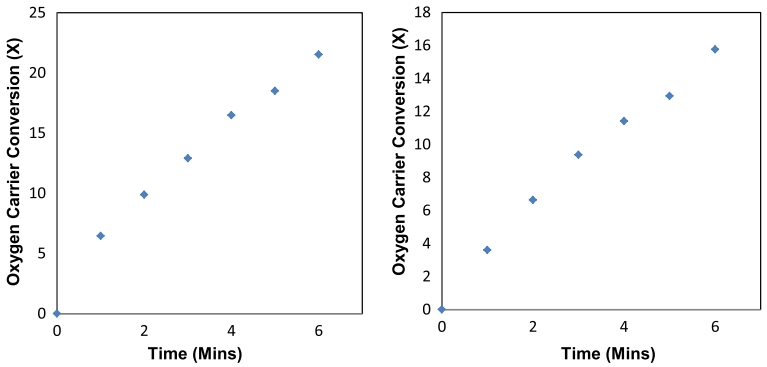

Fig. 4 Experimental result for rate of oxygen carrier conversion for CuO/Nb_2O_5 powder on left and pellets on the right performed at 800 °C for a period of 6 min

in chemical looping are pure materials of CuO/CeO_2 and CuO/Nb_2O_5 oxygen carriers.

Reactivity studies

The reactivity of the oxygen carriers were studied using a fixed bed reactor with 12 mm internal diameter and 40 mm length in which 3 g of the oxygen carriers were placed in the reactor between coarse sand and the temperature of operation was 800 °C. The oxygen carrier conversions for 6 min of operation were plotted against time as indicated in Fig. 3 for CuO/CeO_2 oxygen carrier powder and pellets while that of CuO/Nb_2O_5 oxygen carrier powder and pellets is shown in Fig. 4.

The results in Figs. 3 and 4 shows that the rate of conversion of oxygen carrier is higher for the carriers in powder forms compared to those in pellets forms. This can be as a result of surface area for reaction which is higher for oxygen carrier powder

compared to those of pellets. There may also be mass transfer effect that contributes to the resistance in pellets [59] which may lead to their conversion being lower.

Models were selected from those presented in Table 1 and plotted using expressions presented in the table for each of the oxygen carriers to obtain the model that exhibit the best fit by comparing the correlations (R^2) of the various models and determining their errors. The best model is expected to maximize the correlation and minimize both the standard and the sum of squares errors. The plots are shown in Figs. 5, 6, 7, and 8 for CuO/CeO_2 oxygen carrier powder, CuO/CeO_2 oxygen carrier pellets, CuO/Nb_2O_5 oxygen carrier powder and CuO/Nb_2O_5 oxygen carrier pellets.

Fig. 5 shows that the model with the highest correlation is first order kinetics model while three dimensional contraction model has the best correlation as shown on Fig. 6 which is an indication that those models can best be used to describe the kinetics of the oxygen carrier reactions. The first order kinetics of the powder form of oxygen carrier is due to abundance of oxygen in the oxygen carrier [30] that will readily react with the fuel thereby making all other resistances negligible. As for the contraction model of the pellets form of the oxygen carrier, the size of the pellets make it difficult for the release of oxygen by the oxygen carrier which therefore leads to the shrinking of the core of the oxygen carrier as the gas reacts with the vacant oxygen on the surface of the sphere. For CuO/Nb_2O_5 oxygen carrier (Figs. 7 and 8), it can be seen that the model with best correlation is third order kinetics model for both powder and pellets form of the oxygen carrier. This is an indication that the reaction is kinetics control which is non-linear and there is no any other resistance controlling the reaction between the oxygen carrier and the fuel.

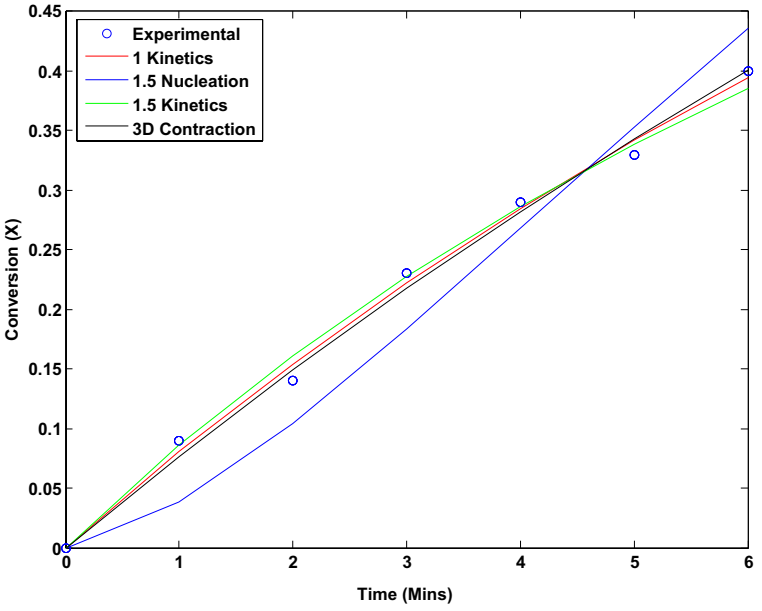

Fig. 5 Rate of conversion for different models (solid lines) as presented on the legend as well as the experimental values (°) for CuO/CeO_2 oxygen carrier powder

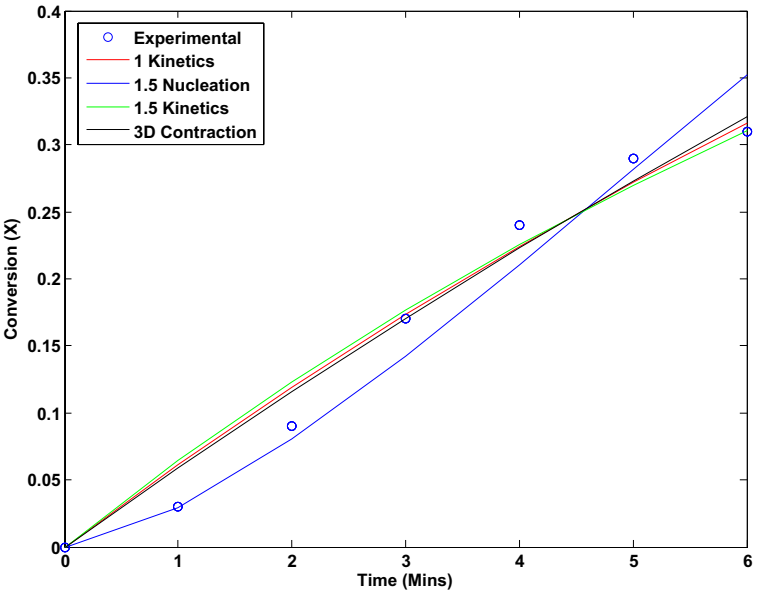

Fig. 6 Rate of conversion for different models as presented on the legend as well as the experimental values (°) for CuO/CeO_2 oxygen carrier pellets

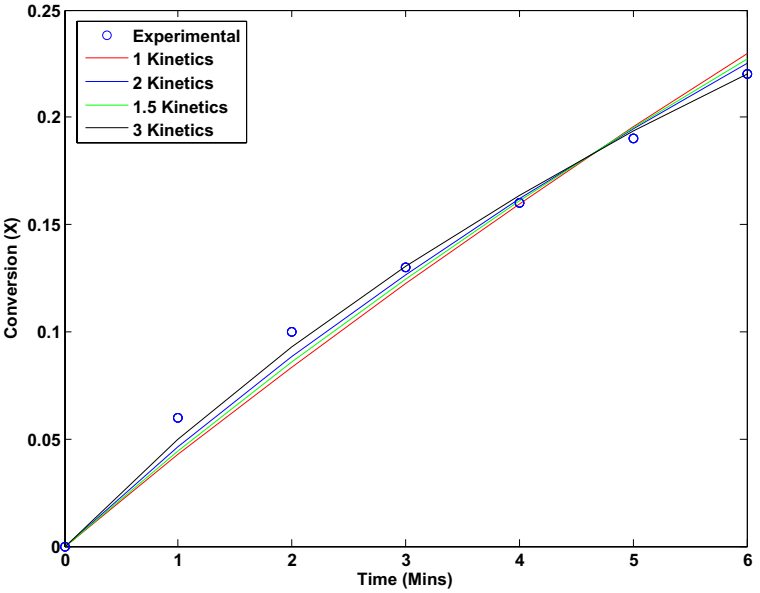

Fig. 7 Rate of conversion for different models as presented on the legend as well as the experimental values (°) for CuO/Nb_2O_5 oxygen carrier powder

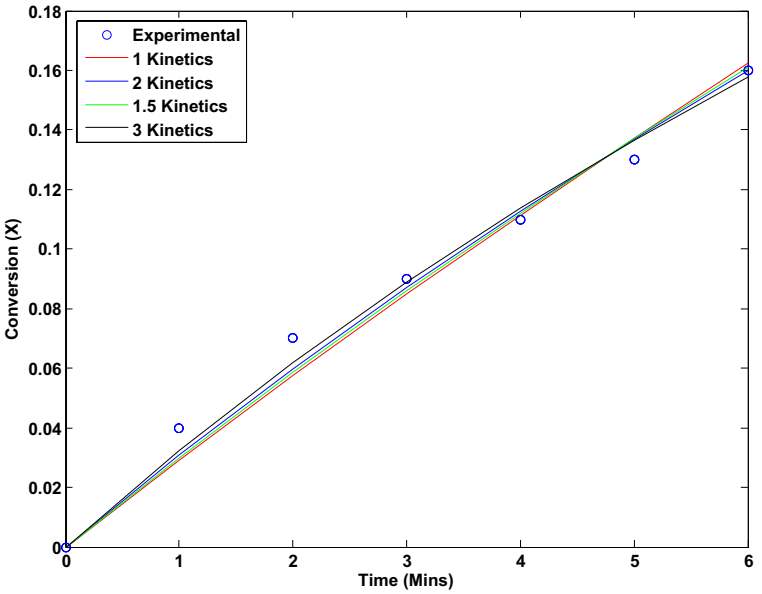

Fig. 8 Rate of conversion for different models as presented on the legend as well as the experimental values (°) for CuO/Nb_2O_5 oxygen carrier pellets

Using the models with the best fits, the slopes obtained from the plots are the rate constants (k(T)) which are 0.0837 s^{-1} for CuO/CeO_2 oxygen carrier powder, 0.0202 s^{-1} for CuO/CeO_2 oxygen carrier pellets, 0.1075 s^{-1} for CuO/Nb_2O_5 oxygen carrier powder and 0.0682 s^{-1} for CuO/Nb_2O_5 oxygen carrier pellets. Since the rate of conversion of the oxygen carrier is directly proportional to the rate constant as shown in Eq. 1, this implies that the higher the value of the rate constant, the higher the conversion rate. Consequently, the conversion rates of the oxygen carriers in powder form are higher than those of the pellets as confirmed by the conversion rates shown in Figs. 3 and 4.

The validity of the models can be evaluated statistically by examining the errors in using the selected models. The standard error (SE) was evaluated using Eq. 10 while sum of squares error (SSE) was evaluated using the expression presented by Lente (2015) [47] and the results obtained are presented in Table 2.

Table 2 Statistical data and rate constant values k for the selected models

Oxygen carrier	Model	k	R^2	SE	SSE
CuO/CeO_2 powder	First order kinetic	0.0837	0.9954	0.0019	0.0006
CuO/CeO_2 pellets	3D contraction	0.0202	0.9760	0.0126	0.0022
CuO/Nb_2O_5 Powder	Third order kinetic	0.1075	0.9947	0.0103	0.0002
CuO/ Nb_2O_5 pellets	Third order kinetic	0.0682	0.9897	0.0091	0.0002

From Table 2, the values of the correlations are observed to be very high with the minimum of 0.9760 for CuO/CeO_2 Pellets which are indications that the developed models agree with the experimental data, which is further confirmed from the low values of the standard errors and the sum of squares error (SSE) with the highest value being 0.0126 and 0.0022, respectively, which are equivalent to 1.26% and 0.22% SE and SSE, respectively, which are all for CuO/CeO_2 Pellets.

Using the rate constants in the integrated forms of the models, the relationship between conversion and time can be obtained for each of the oxygen carriers. This can be used for the validation of the model by plotting the model output together with the experimental data which was done by developing a code for the plot in MATLAB which can be used as models for each of the oxygen carriers and the plots are as shown in Fig. 9.

From Fig. 9, it can be seen that there is a close correlation between the model and the experimental data with negligible error which can be seen from the closeness of the experimental data to the model lines for each of the oxygen carriers.

Conclusion

From the study which was aimed at establishing a kinetic model for oxygen carrier conversion in chemical looping reforming, it was discovered that using CuO/CeO_2 oxygen carrier and CuO/Nb_2O_5 oxygen carrier, the powder form of the oxygen carrier were found to have higher rate of conversion of the oxygen

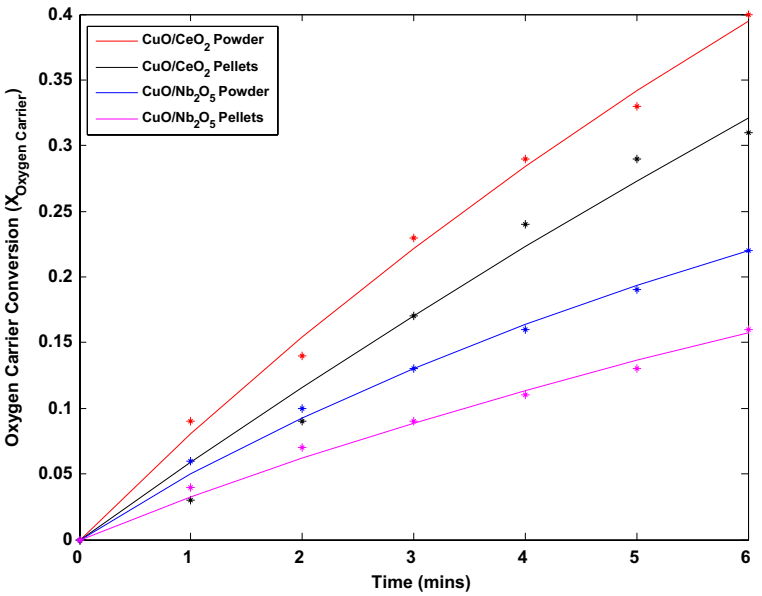

Fig. 9 Selected models rate of oxygen carrier conversions (solid lines) for the various oxygen carriers as shown on the legend compared with their experimental data (*)

carrier where CuO/CeO_2 oxygen carrier powder was found to have a conversion of around 40% after 6 min compared to that of pellets which was around 31% for the same period. Meanwhile for CuO/Nb_2O_5 oxygen carrier, the conversion of the powder oxygen carrier was found to be around 21% which is higher than that of pellets which was found to be around 16% for the same period of 6 min. Among the models tested, first order kinetics was found to give best fit for CuO/CeO_2 oxygen carrier powder with rate constant of 0.0836 s^{-1} and 3D contraction model was found to give best fit for CuO/CeO_2 oxygen carrier pellets with rate constant of 0.0202 s^{-1}, meanwhile for CuO/Nb_2O_5 oxygen carrier, the best fit was obtained using 3rd order kinetic model for both powder and pellets with rate constants of 0.1075 s^{-1} and 0.0682 s^{-1} for powder and pellets, respectively. To validate the model, the model result show close correlation when compared with the experimental data with slight error, which was found to be around 1.26% and 0.22% for SE and SSE which are all for CuO/CeO_2 oxygen carrier pellets.

Acknowledgements I am very grateful to Petroleum Technology Development Fund (PTDF), Nigeria providing the fund needed to carry out the research work, and also Dr. A. Atta for his assistance in analyses of the product gases.

Declarations

Conflict of interest The authors declare that there is no any financial interest that will in any way affect the outcome of this study.

References

1. Lu C, Li K, Wang H, Zhu X, Wei Y, Zheng M, Zeng C (2018) Chemical looping reforming of methane using magnetite as oxygen carrier: Structure evolution and reduction kinetics. Appl Energy 211:1–14. https://doi.org/10.1016/j.apenergy.2017.11.049
2. Forutan HR, Karimi E, Hafizi A, Rahimpour MR, Keshavarz P (2015) Expert representation chemical looping reforming: A comparative study of Fe, Mn, Co and Cu as oxygen carriers supported on Al 2 O 3. J Ind Eng Chem 21:900–911. https://doi.org/10.1016/j.jiec.2014.04.031
3. He F, Wei Y, Li H, Wang H (2009) Synthesis gas generation by chemical-looping reforming using Ce-based oxygen carriers modified with Fe, Cu, and Mn oxides. Energy Fuels 23(4):2095–2102. https://doi.org/10.1021/ef800922m
4. Shahbaz M, Yusup S, Inayat A, Patrick DO, Pratama A, Ammar M (2017) Optimization of hydrogen and syngas production from PKS gasification by using coal bottom ash. Biores Technol 241:284–295. https://doi.org/10.1016/j.biortech.2017.05.119
5. Velasco JA, Lopez L, Velásquez M, Boutonnet M, Cabrera S, Järås S (2010) Gas to liquids: a technology for natural gas industrialization in Bolivia. J Nat Gas Sci Eng 2(5):222–228. https://doi.org/10.1016/j.jngse.2010.10.001
6. Gu Z, Li K, Wang H, Wei Y, Yan D, Qiao T (2013) Syngas production from methane over CeO2-Fe2O3 mixed oxides using a chemical-looping method. Kinet Catal 54(3):326–333. https://doi.org/10.1134/S002315841303004X
7. Genovese NA, Gorlani A, Arroyo PAH (2005) GTL technology and it's role in the world energy markets. Scuola Mattei.
8. Wang P, Howard B, Means N, Shekhawat D, Berry D (2019) Coal chemical-looping with oxygen uncoupling (CLOU) using a Cu-based oxygen carrier derived from natural minerals. Energies 12(8):1453. https://doi.org/10.3390/en12081453

9. Zhang J, Zhao N, Wei W, Sun Y (2010) Partial oxidation of methane over Ni/Mg/Al/La mixed oxides prepared from layered double hydrotalcites. Int J Hydrogen Energy 35(21):11776–11786. https://doi.org/10.1016/j.ijhydene.2010.08.025
10. Li D, Xu R, Gu Z, Zhu X, Qing S, Li K (2020) Chemical-looping conversion of methane: a review. Energ Technol 8(8):1900925. https://doi.org/10.1002/ente.201900925
11. Ismail OS, Umukoro GE (2016) Modelling combustion reactions for gas flaring and its resulting emissions. J King Saud Univ Eng Sci 28(2):130–140. https://doi.org/10.1016/j.jksues.2014.02.003
12. Chen Y-Y, Nadgouda S, Shah V, Fan L-S, Tong A (2020) Oxidation kinetic modelling of Fe-based oxygen carriers for chemical looping applications: Impact of the topochemical effect. Appl Energy 279:115701. https://doi.org/10.1016/j.apenergy.2020.115701
13. Huang J, Liu W, Hu W, Metcalfe I, Yang Y, Liu B (2019) Phase interactions in Ni-Cu-Al2O3 mixed oxide oxygen carriers for chemical looping applications. Appl Energy 236:635–647. https://doi.org/10.1016/j.apenergy.2018.12.029
14. Li K, Wang H, Wei Y (2013) Syngas generation from methane using a chemical-looping concept: a review of oxygen carriers. J Chem. https://doi.org/10.1155/2013/294817
15. Khan MN, Shamim T (2017) Thermodynamic screening of suitable oxygen carriers for a three reactor chemical looping reforming system. Int J Hydrogen Energy 42(24):15745–15760. https://doi.org/10.1016/j.ijhydene.2017.05.037
16. Kang K-S, Kim C-H, Bae K-K, Cho W-C, Kim S-H, Park C-S (2010) Oxygen-carrier selection and thermal analysis of the chemical-looping process for hydrogen production. Int J Hydrogen Energy 35(22):12246–12254. https://doi.org/10.1016/j.ijhydene.2010.08.043
17. Yan Y, Xu L, Wang L, Fu K, Tang M, Fan M, Ma X (2018) Syngas Production from chemical-looping reforming of methane using iron-doped cerium oxides. Energ Technol 6(9):1610–1617. https://doi.org/10.1002/ente.201700884
18. Adnan MA (2020) Integrated diesel fueled chemical looping combustion for power generation and CO2 capture – performance evaluation based on exergy analysis. *Energy Conv Manag* 11.
19. Bhavsar S, Veser G (2014) Chemical looping beyond combustion: production of synthesis gas via chemical looping partial oxidation of methane. RSC Adv 4:47254–47267. https://doi.org/10.1039/C4RA06437B
20. Han L, Zhou Z, Bollas GM (2016) Model-based analysis of chemical-looping combustion experiments. Part II: optimal design of CH4-NiO reduction experiments. *AIChE J 62*(7), 2432–2446.
21. Wang Y, Zheng Y, Wang Y, Li K, Wang Y, Jiang L, Wei Y, Wang H (2019) Syngas production modified by oxygen vacancies over CeO2-ZrO2-CuO oxygen carrier via chemical looping reforming of methane. Appl Surf Sci 481:151–160. https://doi.org/10.1016/j.apsusc.2019.03.050
22. Yang J, Wei Y, Yang J, Xiang H, Ma L, Zhang W, Wang L, Peng Y, Liu H (2019) Syngas production by chemical looping gasification using Fe supported on phosphogypsum compound oxygen carrier. Energy 168:126–135. https://doi.org/10.1016/j.energy.2018.11.106
23. Yan Y, Mattisson T, Moldenhauer P, Anthony EJ, Clough PT (2020) Applying machine learning algorithms in estimating the performance of heterogeneous, multi-component materials as oxygen carriers for chemical-looping processes. Chem Eng J 387:124072. https://doi.org/10.1016/j.cej.2020.124072
24. Lyngfelt A (2013) Chemical looping combustion (CLC). In *Fluidized Bed Technologies for Near-Zero Emission Combustion and Gasification* (pp. 895–930). Elsevier. https://doi.org/10.1533/9780857098801.4.895
25. Zeng L, He F, Li F, Fan L-S (2012) Coal-direct chemical looping gasification for hydrogen production: reactor modeling and process simulation. Energy Fuels 26(6):3680–3690. https://doi.org/10.1021/ef3003685
26. Luo S, Zeng L, Fan L-S (2015) Chemical looping technology: oxygen carrier characteristics. Annu Rev Chem Biomol Eng 6(1):53–75. https://doi.org/10.1146/annurev-chembioeng-060713-040334
27. Aghabararnejad M, Patience GS, Chaouki J (2014) TGA and kinetic modelling of Co, Mn and Cu oxides for chemical looping gasification (CLG). Canadian J Chem Eng 92(11):1903–1910. https://doi.org/10.1002/cjce.22046
28. Arjmand M, Leion H, Mattisson T, Lyngfelt A (2013) ZrO2-supported CuO oxygen carriers for chemical-looping with oxygen uncoupling (CLOU). Energy Procedia 37:550–559. https://doi.org/10.1016/j.egypro.2013.05.141
29. Zhao H, Guo L, Zou X (2015) Chemical-looping auto-thermal reforming of biomass using Cu-based oxygen carrier. Appl Energy 157:408–415. https://doi.org/10.1016/j.apenergy.2015.04.093

30. Monazam ER, Breault RW, Tian H, Siriwardane R (2015) Reaction kinetics of mixed CuO–Fe $_2$ O $_3$ with methane as oxygen carriers for chemical looping combustion. Ind Eng Chem Res 54(48):11966–11974. https://doi.org/10.1021/acs.iecr.5b02848
31. Fang H, Haibin L, Zengli Z (2009) Advancements in development of chemical-looping combustion: a review. Int J Chem Eng 2009:1–16. https://doi.org/10.1155/2009/710515
32. Fan L-S, Zeng L, Luo S (2015) Chemical-looping technology platform. AIChE J 61(1):2–22. https://doi.org/10.1002/aic.14695
33. Li F, Zeng L, Velazquez-Vargas LG, Yoscovits Z, Fan L-S (2010) Syngas chemical looping gasification process: Bench-scale studies and reactor simulations. AIChE J 56(8):2186–2199. https://doi.org/10.1002/aic.12093
34. Otsuka K, Wang Y, Nakamura M (1999) Direct conversion of methane to synthesis gas through gas–solid reaction using CeO2–ZrO2 solid solution at moderate temperature. Appl Catal A 183(2):317–324. https://doi.org/10.1016/S0926-860X(99)00070-8
35. Liu F (2013) Cerium oxide (CeO2) promoted oxygen carrier development and scale modeling study for chemical looping combustioN (Doctor of Philosophy). University of Kentucky, Lexington, Kentucky
36. Wei Y, Wang H, He F, Ao X, Zhang C (2007) CeO2 as the oxygen carrier for partial oxidation of methane to synthesis gas in molten salts: thermodynamic analysis and experimental investigation. J Nat Gas Chem 16(1):6–11. https://doi.org/10.1016/S1003-9953(07)60018-8
37. Li K, Wang H, Wei Y, Yan D (2010) Direct conversion of methane to synthesis gas using lattice oxygen of CeO2–Fe2O3 complex oxides. Chem Eng J 156(3):512–518. https://doi.org/10.1016/j.cej.2009.04.038
38. Li K, Wang H, Wei Y, Yan D (2011) Transformation of methane into synthesis gas using the redox property of Ce–Fe mixed oxides: Effect of calcination temperature. Int J Hydrogen Energy 36(5):3471–3482. https://doi.org/10.1016/j.ijhydene.2010.12.038
39. dos Santos PHLNA, Nowak S, Lau-Truong S, Blanchard J, Beaunier P, Rodrigues JAJ, Brayner R (2019) Preparation of niobium-based oxygen carriers by polyol-mediated process and application to chemical-looping reforming. J Nanopart Res 21(5):1–16. https://doi.org/10.1007/s11051-019-4528-z
40. Yaremchenko AA, Kharton VV, Veniaminov SA, Belyaev VD, Sobyanin VA, Marques FMB (2007) Methane oxidation by lattice oxygen of CeNbO4+δ. Catal Commun 8(3):335–339. https://doi.org/10.1016/j.catcom.2006.07.004
41. Wei Y, Wang H, Li K, Zhu X, Du Y (2010) Preparation and characterization of Ce1-x NixO2 as oxygen carrier for selective oxidation methane to syngas in absence of gaseous oxygen. J Rare Earths 28:357–361. https://doi.org/10.1016/S1002-0721(10)60358-4
42. Means NC, Burgess WA, Howard BH, Smith MW, Wang P, Shekhawat D (2019) Examining and modeling oxygen uncoupling kinetics of Cu-based oxygen carriers for chemical looping with oxygen uncoupling (CLOU) in a drop tube fluidized bed reactor. Energy Fuels 33(6):5610–5619. https://doi.org/10.1021/acs.energyfuels.9b00338
43. Naji A (2011) Kinetic study of chemical looping combustion using iron as an oxygen carrier (Masters). Dalhousie University Halifax, Nova Scotia
44. Go K, Son S, Kim S (2008) Reaction kinetics of reduction and oxidation of metal oxides for hydrogen production. Int J Hydrogen Energy 33(21):5986–5995. https://doi.org/10.1016/j.ijhydene.2008.05.039
45. Monazam ER, Breault RW, Siriwardane R, Richards G, Carpenter S (2013) Kinetics of the reduction of hematite (Fe2O3) by methane (CH4) during chemical looping combustion: a global mechanism. Chem Eng J 232:478–487. https://doi.org/10.1016/j.cej.2013.07.091
46. Lente G (2018) Facts and alternative facts in chemical kinetics: remarks about the kinetic use of activities, termolecular processes, and linearization techniques. Curr Opin Chem Eng 21:76–83. https://doi.org/10.1016/j.coche.2018.03.007
47. Lente G (2015) Deterministic kinetics in chemistry and systems biology. Springer International Publishing, Cham
48. Bhavsar S, Veser G (2013) Bimetallic Fe–Ni oxygen carriers for chemical looping combustion. Ind Eng Chem Res 52:15342–15352. https://doi.org/10.1021/ie400612g
49. Cho P (2005) Development and characterisation of oxygen-carrier materials for chemical-looping combustion. Chalmers University of Technology, Göteborg

50. Liu F, Chen L, Neathery JK, Saito K, Liu K (2014) Cerium oxide promoted iron-based oxygen carrier for chemical looping combustion. Ind Eng Chem Res 53(42):16341–16348. https://doi.org/10.1021/ie503160b
51. Chen S, Soomro A, Yu R, Hu J, Sun Z, Xiang W (2018) Integration of chemical looping combustion and supercritical CO2 cycle for combined heat and power generation with CO2 capture. Energy Convers Manage 167:113–124. https://doi.org/10.1016/j.enconman.2018.04.083
52. Adanez J, Abad A, Garcia-Labiano F, Gayan P, de Diego LF (2012) Progress in chemical-looping combustion and reforming technologies. Prog Energy Combust Sci 38(2):215–282. https://doi.org/10.1016/j.pecs.2011.09.001
53. Chen C, Bollas GM (2020) Design and scheduling of semibatch chemical-looping reactors. Ind Eng Chem Res 59(15):6994–7006. https://doi.org/10.1021/acs.iecr.9b05693
54. Lu C, Deng R, Xu R, Zhao Y, Zhu X, Wei Y, Li K (2021) Design of hybrid oxygen carriers with CeO2 particles on MnCo2O4 microspheres for chemical looping combustion. Chem Eng J 404:126554. https://doi.org/10.1016/j.cej.2020.126554
55. Solsona B, Sanchis R, Dejoz A, García T, Ruiz-Rodríguez L, López Nieto J, Cecilia J, Rodríguez-Castellón E (2017) Total oxidation of propane using CeO2 and CuO-CeO2 catalysts prepared using templates of different nature. Catalysts 7(12):96. https://doi.org/10.3390/catal7040096
56. Chary KVR, Seela KK, Sagar GV, Sreedhar B (2004) Characterization and reactivity of niobia supported copper oxide catalysts. J Phys Chem B 108(2):658–663. https://doi.org/10.1021/jp035738s
57. Braga V, Garcia F, Dias J, Dias S (2007) Copper oxide and niobium pentoxide supported on silica-alumina: Synthesis, characterization, and application on diesel soot oxidation. J Catal 247(1):68–77. https://doi.org/10.1016/j.jcat.2006.12.022
58. Djinović P, Batista J, Pintar A (2008) Calcination temperature and CuO loading dependence on CuO-CeO2 catalyst activity for water-gas shift reaction. Appl Catal A 347(1):23–33. https://doi.org/10.1016/j.apcata.2008.05.027
59. Saucedo MA, Dennis JS, Scott SA (2015) Modelling rates of gasification of a char particle in chemical looping combustion. Proc Combust Inst 35(3):2785–2792. https://doi.org/10.1016/j.proci.2014.07.005